Daniela Medas, Giovanni De Giudici, Maria Antonietta Casu, Elodia Musu, Alessandra Gianoncelli, Antonella Iadecola, Carlo Meneghini, Elena Tamburini, Anna Rosa Sprocati, Katarzyna Turnau, and Pierfranco Lattanzi (2015). Microscopic processes ruling the bioavailability of Zn to roots of Euphorbia pithyusa L. Pioneer plant. Environmental Science and Technology, 49(3), 1400–1408. https://doi.org/10.1021/es503842w

Microscopic processes ruling Zn bioavailability to roots of *Euphorbia pithyusa* L. pioneer plant.

Daniela Medas [a], Giovanni De Giudici,* [a] Maria Antonietta Casu [b], Elodia Musu [c], Alessandra Gianoncelli [d], Antonella Iadecola [d], Carlo Meneghini [e], Elena Tamburini [f], Anna Rosa Sprocati [g], Katarzyna Turnau [h], Pierfranco Lattanzi [a]

[a] Department of Chemical and Geological Sciences, University of Cagliari, 09127 Cagliari, Italy
[b] National Research Council, Institute of Translational Pharmacology, UOS of Cagliari, Scientific and Technological Park of Sardinia POLARIS, Pula, Italy
[c] Sardegna Ricerche/CRS4–Telemicroscopy Lab, Scientific and Technological Park of Sardinia POLARIS, Pula, Italy
[d] Elettra-Sincrotrone Trieste, Area Science Park, Basovizza, Trieste, Italy
[e] Physics Department, University of Roma Tre, 00146 Rome, Italy
[f] Department of Biomedical Science, University of Cagliari, Cittadella Universitaria, 09042 Monserrato, Cagliari, Italy
[g] Environmental Characterization, Prevention and Recovery Unit,ENEA-Casaccia, Rome, Italy
[h] Institute of Environmental Sciences of the Jagiellonian University, Gronostajowa 7, 30-387 , Kraków, Poland

Abstract

Euphorbia pithyusa L. was used in a plant-growth-promoting assisted field trial experiment. In order to unravel the microscopic processes at the interface, thin slices of *E. pithyusa* roots were investigated by micro-X-ray fluorescence mapping (μ-XRF). Roots and rhizosphere materials were examined by X-ray absorption spectroscopy (XAS) at the Zn K-edge, by X-ray Diffraction (XRD), and Scanning Electron Microscopy (SEM).

Results indicate some features common to all the investigated samples: i) in the rhizosphere of *E. pithyusa* Zn was found to occur in different phases; ii) Si and Al are mainly concentrated in the epidermis of the roots forming a rim; iii) Zn is mostly stored in root epidermis, and does not appear coordinated to organic molecules, but mainly occurring in mineral phases such as Zn-silicates.

We interpreted that roots of *E. pithyusa* significantly promote mineral evolution in the rhizosphere. Concomitantly, the plant uses Si and Al extracted by soil minerals to build a biomineralization rim, which is able to capture Zn. This Zn-silicate biomineralization has relevant implication for phytoremediation techniques and for further biotechnology development, which can be better designed and developed after acquiring specific knowledge of molecular processes ruling mineral evolution and biomineralization processes.

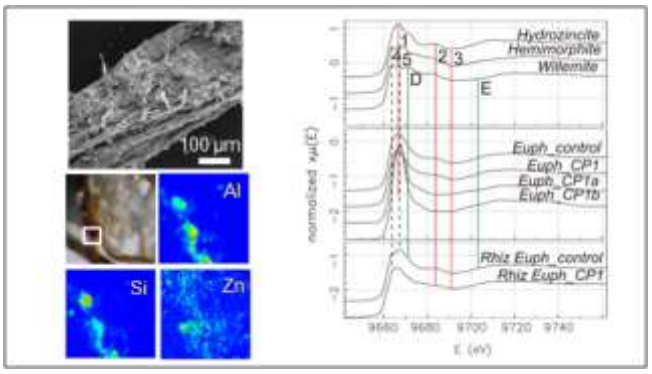

Keywords: Plant biomineralization, *Euphorbia pithyusa*, STXM, XAS, silicon, aluminium, zinc, iron, synchrotron radiation based X-ray analysis

1. Introduction

Biomineralization in plants is part of a complex interaction process involving soil minerals, plant-roots, and plant-associated microorganisms. It results from metabolic functioning of a living organism, and is widely practiced by plants for many physiological purposes, both within and outside the cells.[1,2] Biomineralization in plants can play diverse roles, such as Ca-regulation, defence against predators, alleviating water, salt, and temperature stress, and detoxifying from aluminium, heavy metals, or oxalic acid. [3,4] The most common types of biominerals in plants are

Ca-oxalates, Ca-carbonates, and silica.[3] In addition, a few biominerals containing heavy metals were observed, generally interpreted as a response to specific environmental stress. [5-9] Moreover, microscopic processes and biomineralization are relevant to phytoremediation techniques, because they rule element bioavailability,[10] namely leaching from minerals, accumulation of elements inside the roots or in the rhizosphere, and then, depending on the physiological system, translocation to upper compartments of the plants,[11-14] or metal immobilization into the soil or within plant roots.[15]

In the frame of the EU-funded UMBRELLA project, a field trial of microbial-assisted plant growth was carried out in the mining area of Ingurtosu (SW Sardinia, Italy). *E. pithyusa* was selected as an autochthonous pioneer plant in mine wastes to be associated with a consortium of ten selected native bacteria strains plus/or with mycorrhiza.[16] It is well known that bioremediation technologies are slow and that, before observing some relevant effect, the complex system of interactions between plant soil and microorganisms needs some time (years) to be established.[17,18] However, some parameters are early indicators of what is (or is not) occurring, and provide useful methodological guidance to orient experimentation. Changes in metabolic activity of the soil were considered in Sprocati et al.,[16] while in the present work we explore geo-biological processes occurring at the root-soil interface.

The study made extensive use of synchrotron-based techniques.[19,20] Specifically, elemental distribution was investigated by Synchrotron micro-X-ray fluorescence (μ-XRF) imaging, and chemical speciation of Zn was examined by X-ray absorption spectroscopy (XAS). In addition, X-ray Diffraction (XRD), and Scanning Electron Microscopy (SEM) were used to investigate mineralogical and morphological features. Previous works based on Synchrotron techniques found that Zn speciation in plant roots is ruled by complexation with organic molecules;[21-24] Zn binding to Si can rarely occur[25] in plant leaves. In this work we will show that Zn bioavailability at *E. pithyusa* roots can be ruled by Zn-silicate phase formation. Acquiring knowledge of these molecular scale processes opens the way to a new perspective for phytoremediation and biotechnology.

2. Materials and methods

2.1 The field experimental trial and samples characteristics

In the Ingurtosu mining district, near the Brassey treatment plant (see SI S1 for additional information on sampling area), an area of about 7.5 m×22.5 m (Figure S1a) on the mine dump was levelled, and then divided into 27 subplots. Soil subplots were treated with different materials, supplied singly or in combination. In this study we consider subplots added with a bacterial consortium,[26] and/or mycorrhizae. For this purpose, microbial strains with suitable characteristics, heavy-metal (HM) tolerant and plant – growth - promoters (PGP), were selected to establish microbial consortia to be employed as bioaugmentation agents in phytoremediation experiments. Mycorrhizae contribution was also investigated: mycorrhiza dependence is common among plants selected for phytoremediation of industrial tailings.[27] Moreover, some subplots were added with a commercial mineral amendment (Viromine™) obtained from "red mud", a by-product of the bauxite industry, which is widely used, after adequate neutralization, for environmental remediation processes due to its metal-trapping capacity;[28-34] these specific plots will be the subject of a companion study. Control plots without treatment were also planted with *E. pithyusa*. The preliminary results of five months of the experiment indicate that plant survival was satisfactory, and soil quality was increased as bioaugmentation improved microbial activity, expanding the metabolic competences towards plant interaction (root exudates; for more details see Sprocati et al.[16]). Grain size and mineralogical composition of the substrate resulted substantially homogeneous for all the subplots. Mine wastes are mainly composed of quartz and illite, with detectable (X-ray powder diffraction) amounts of sphalerite. The most abundant metals are Zn (15,000 mg/kg), Pb (3,400 mg/kg), Cu (350 mg/kg), and Cd (90 mg/kg).

Samples from this study include rhizosphere materials and plant roots collected in the field test area at Ingurtosu, plus additional plants harvested in two areas outside the field trial where they grow spontaneously. Specifically, we selected another mine area at Campo Pisano (see S1 and Figure

S1b), and an area near the village of Fluminimaggiore (SW Sardinia), that lies outside mine areas, even if it is affected by a regional geochemical anomaly in Zn.[35,36]

Different portions of the roots were selected: 1) entire root, 2) epidermis, 3) inner layers (Table 1). Inner layers were selected only for the sample from Campo Pisano mine that has the highest Zn concentration.

Table 1. Sample nomenclature, treatment, location, site and XANES group.

Sample	Type	Treatment	Location	Site
Euph	root	-	External to the mining areas	Fluminimaggiore
Euph_control	root	-	Experimental field (control plot)	Ingurtosu
Euph_A2	root	Bacterial consortium	Experimental field	Ingurtosu
Euph_B1	root	Mycorrhiza	Experimental field	Ingurtosu
Euph_MB	root	Mycorrhiza + Bacterial consortium	Experimental field	Ingurtosu
Euph_CP1	root	-	Mine tailings	Campo Pisano
Euph_CP1a	inner layers	-	Mine tailings	Campo Pisano
Euph_ CP1b	root epidermis	-	Mine tailings	Campo Pisano

Plants were harvested few days before the experiments described in the following paragraphs.

2.2 X-ray Diffraction analysis

After collection of plants, roots were cut and air dried. Approximately 200 mg of each sample were lightly ground in an agate mortar, and analyzed by X-ray diffraction (XRD), using conventional θ-2θ equipment (Panalytical) with Cu K_α wavelength radiation (λ = 1.54060 Å), operating at 40 kV and 40 mA, using the X'Celerator detector.

2.3 Electron Microscopic analysis

Before imaging, plant roots were gently wiped to remove rhizosphere material not stuck to the root surface. SEM imaging and EDX (Energy Dispersive Spectroscopy) analysis were carried out using a field emission (Schottky thermal field emitter) SEM (FEI), under high vacuum conditions. In order to obtain better quality images, samples were gold coated before observation, using a SEM Coating Unit PS3 (Agar Aids for Electron Microscopy).

2.4 Soft X-ray Microscopy and Low Energy Fluorescence Mapping

For soft X-ray Microscopy combined with Low Energy XRF mapping analyses, root samples were prepared by two different procedures. 1) Samples were dehydrated in a graded series of ethanol solutions (50, 75, 90 and 100 %) followed by washing in xylene. All steps were carried out at room temperature for 30 min each. Samples were infiltrated overnight in liquid paraffin wax at 60 °C and the infiltrated roots were then embedded into paraffin blocks. Sections of 14 µm were cut with a microtome (Micron) and collected on ultralen films. 2) Root samples were transferred to a cryomold filled with OCT compound (Optimal Cutting Temperature compound for cryostat sectioning) and frozen at -20°C. Sections of 20 µm were cut with a cryostat (Leica) and collected on gold grids (parallel bar grids, G2010A, and folding grids, G230A) for Transmission Electron Microscopy analysis. Samples were then lyophilized (LIO5P, 5Pascal) under low vacuum conditions and temperature of -50°C (24 hours).

Soft X-ray Microscopy combined with Low Energy XRF mapping analyses were performed at the TwinMic beamline[37] at ELETTRA, Trieste (Italy). The TwinMic microscope was operated in Scanning Transmission mode, where the monochromatised X-rays are focused on the sample through a suitable zone plate diffractive optics. While the sample is raster scan across the microprobe, a fast readout CCD camera (Andor Technology) collects the transmitted X-rays[38,39] through an X-ray-visible light converting system, 8 SDDs[40,41] acquire the XRF photons emitted by the specimen. This set-up allows the simultaneous collection of X-ray absorption and phase contrast images together with elemental maps, providing morphological and chemical information respectively.

For the present investigation, the X-ray beam energy (E = 1.985keV) was chosen to ensure the best excitation and detection of Si, Al, and Zn, with a spatial resolution (X-ray spot size) of 1 µm x 1 µm as a compromise between good XRF signal and dimension of the features of interest.

The XRF elemental maps were deconvolved and analysed with PyMCA software.[42]

2.5 X-Ray Absorption Spectroscopy

X-Ray Absorption Spectroscopy (XAS) experiments were carried out in the region of Zn (9.659 eV) K-edge at the XAFS beamline, ELETTRA, Trieste (Italy), and at the BM23 beamline, ESRF, Grenoble (France). The plant roots were dried, ground, then pressed in solid pellets, suitable for XAS measurements. Measurements were carried out in fluorescence geometry at the liquid nitrogen temperature. The absorption spectra were analysed in the near edge (XANES: near edge X-ray absorption fine structure) and extended (EXAFS: extended X-ray absorption fine structure) regions. The EXAFS spectra were quantitatively analysed using standard data analysis procedures to achieve details about the average atomic structure (coordination distances and numbers) around the absorber. Details about XAS data treatment and refinement procedures can be found in Meneghini et al.[43] and Medas et al.[44]

3. Results

3.1 Mineralogical characterization

Figures S2a and b show XRD patterns of selected plant root samples. Patterns not shown from the Ingurtosu experimental plots are essentially similar to the *Euph_control* sample. All the XRD patterns show the presence of amorphous cellulose, recognizable from the wide peaks at around 14.9-16.5 2θ and 22.8 2θ. Also the peak of quartz at 26.6 2θ (3.343 Å) was observed in all the XRD patterns. Peaks of whewellite [$Ca(C_2O_4)\cdot(H_2O)$] were observed only in the epidermis of root samples from Campo Pisano mine. Whewellite is the monohydrate form of Ca-oxalate, characterized by a low solubility,[45] with a widespread occurrence among bacteria, algae, higher plants, fungi, and animals.[46]

Table 2. Mineralogical composition of rhizosphere solid materials. Qz (quartz), Ph (phyllosilicates), K-fs (K feldspar), Hem (hematite), Cal (calcite), Cer (cerussite), Dol (dolomite), Sp (sphalerite), Py (pyrite), and Ilm (ilmenite).

Sample	Qz	Ph	K-fs	Hem	Cal	Cer	Dol	Sp	Py	Ilm
Rhiz Euph	x	x	x	x						
Rhiz Euph_control	x	x	x		x					
Rhiz Euph_CP1	x	x			x	x	x	x	x	x

Figure S3 shows some selected XRD patterns of rhizosphere solid materials. These are mainly made of quartz (Qz) and phyllosilicates (Ph). Rhizosphere solid materials of *E. pithyusa* from Ingurtosu show homogenous composition, both in absence of any treatment and in treated soils. Table 2 shows the mineralogical composition of selected samples.

3.2 Microscopic investigation

SEM images (Figures S4a and b), acquired on plant roots collected from treated and untreated soil (control plot), show that minerals like phyllosilicates and quartz (see zoom in Figures S4c and d) stick to the root surfaces and, as visually observed, these mineral grains adhere to the plant roots even after vigorous shaking. Probably, this adhesion is due to mineral weathering induced by the organic acids from root exudates.[47]

Figure 1b is a zooming on *Euph* root sample, presented in Figure 1a, that shows the inner part of the root (vascular tissue with the remaining cortical cells in degraded form, centre of the image), and the outer rim of the root. Figure 1c shows an elemental map acquired by SEM collected on the area of Figure 1b. Si and Al are concentrated mainly in the outer rim, whereas the inner part is characterized by a high concentration in C.

Figure 1. a) and b) Scanning Electron Microscopy (SEM) images (secondary electrons, SE) of Euph sample, and c) elemental map acquired by SEM. Si and Al are concentrated mainly in the root epidermis, whereas the inner part (vascular tissue with the remaining degraded cortical cells) is characterized by a high concentration in C.

3.3 Element distribution and speciation

In Figure 2 three different kinds of images are reported: i) ordinary light stereo-microscope image; ii) bright field (absorption) image; iii) LEXRF maps of Al, Si, Zn and Fe. In the stereo-microscope images, root epidermis appears as a dark brown rim, while the inner part has a light brown colour, and is characterized by a honeycomb-like arrangement. Localization of the elements in these cross sections using LEXRF showed that Al and Si are mainly localized in the root epidermis (Figure 2), whereas Zn and Fe are localized also in the inner part of the plant root, showing a general decrease in concentration from the root rim towards the internal part.

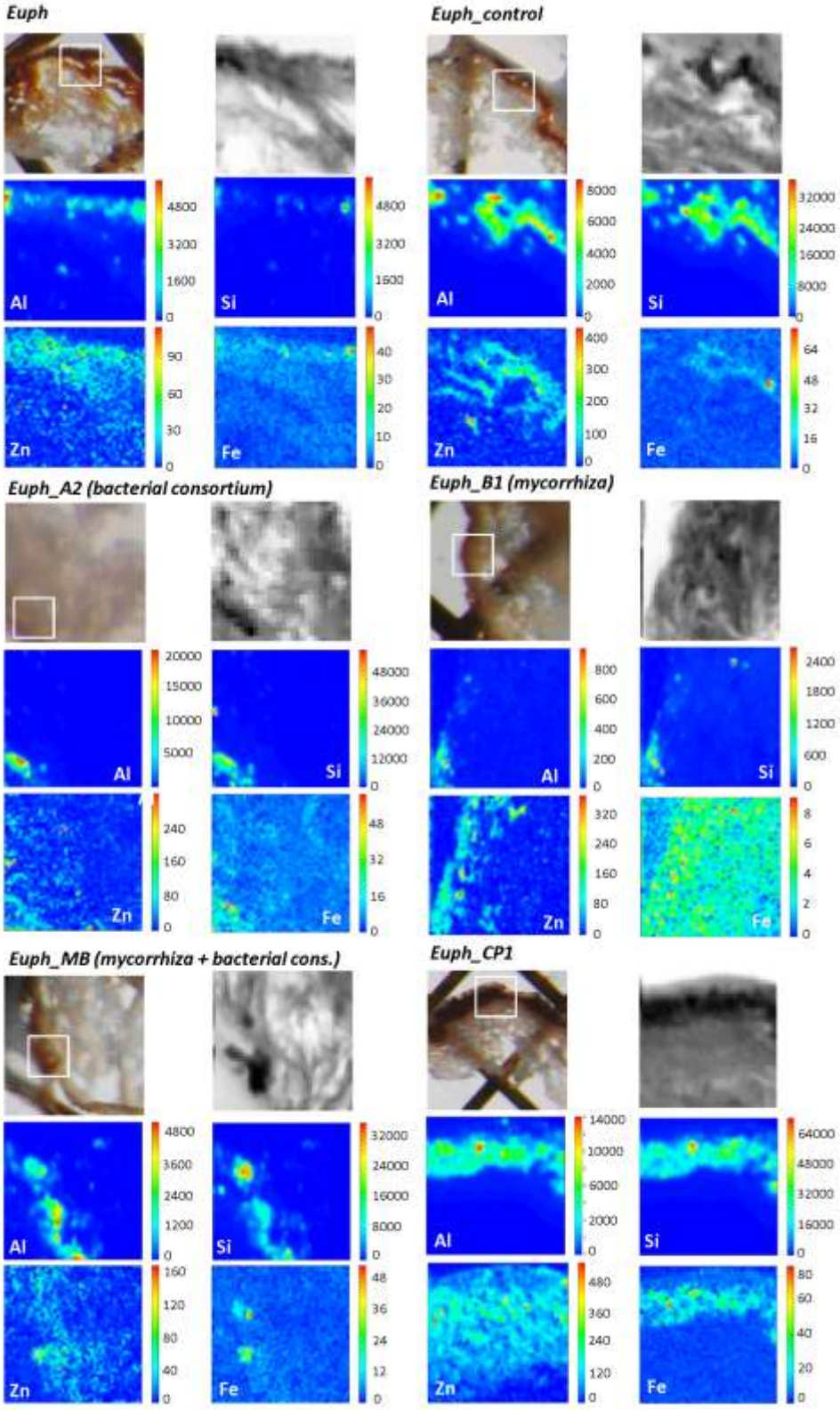

Figure 2. Selected samples of *E. pithyusa*. For each sample the following images are shown: i) ordinary light stereo-microscope image; ii) bright field (absorption) image; iii) LEXRF maps of Al, Si, Zn and Fe (size 80 × 80 µm², scan 80 × 80 pixels).

206 Figures 3a-c report normalized Zn K-edge absorption spectra in the XANES region of selected
207 reference compounds and selected plant root and rhizosphere samples.
208 The analysis of XAS data exploited XANES and EXAFS information. The XANES features may
209 provide finest details about valence state, coordination chemistry and local site symmetry of the
210 average absorber. Unfortunately the quantitative analysis of the XANES regions is generally a
211 difficult task, especially dealing with natural samples. Nevertheless, comparing the Zn K-edge
212 XANES in roots with those of reference compounds is a relatively simple and reliable way to shed
213 light about the average mineralogical environment of the absorber. The set of reference compounds
214 measured for this work (in transmission geometry at room temperature) is listed in Table S1; all
215 XANES spectra of these reference compounds are shown in Figure S5 (Supporting Information).
216 Based on the main XANES spectral features of samples, in comparison with those of reference
217 compounds, it is possible to distinguish four different kinds of spectra, suggesting four different
218 local structure around Zn in the investigated samples. 1) *Euph* spectrum; 2) *Euph_control, A2, B1,*
219 *MB,* and *Euph_CP1* spectra; 3) *Euph_CP1a* spectrum, and 4) *Euph_CP1b* spectrum. Noticeably,
220 most of the investigated samples depict type 2-XANES features, and were considered in the same
221 group. In Figure 3b we show as representatives of this group only the spectrum of *Euph_control*,
222 and the spectrum of plant roots collected at Campo Pisano mine (*Euph_CP1)*. Looking at the Figure
223 3 the XANES spectral features measured from root samples are smoother and broader than in the
224 reference compounds, pointing out a more disordered environment with respect to reference
225 compounds. Interestingly, comparing the XANES features of root samples with those measured in
226 the rhizosphere, similar features can be recognized, pointing out a similar local atomic environment
227 for Zn in the roots and in the surrounding soil.
228 Comparing the Zn XANES features of *Euph* sample with those of the reference compounds, the
229 analogies with the Zn oxide spectrum are quite evident (Figures 3a and b). Specifically, the XANES
230 features labelled as A, B and C in the Zn oxide spectrum are weaker but evidently present also in
231 the spectra of the *Euph* sample, although they are smoothed here by the larger disorder of the root

sample. Similar features are also evident in the spectrum of the rhizosphere sample. This suggests that in this sample a relatively large fraction of Zn is forming a ZnO phase; interestingly, a similar high concentration of ZnO is also evident in the corresponding rhizosphere sample, suggesting the plant directly absorbs Zn in the mineral form already present in the surrounding environment rather than dissolving it. Unfortunately the large fraction of ZnO in this sample masks most of the structural features of Zn in the other phases, moreover the Zn concentration in this *Euph* sample is very low, requiring a very long acquisition time for collecting data of the required statistics also in the EXAFS region. Therefore, we decided to not extend the data acquisition for this sample to the EXAFS region.

The *Euph_control* and *Euph_CP1* XANES depict main spectral features similar to hydrozincite (Figures 3b, labels 1, 2 and 3) with a contribution similar to hemimorphite/willemite (Figures 3b, label 4). *Euph_CP1a* sample (inner root) and *Euph_CP1b* sample (root epidermis) show distinctive characteristics from the other samples and between them. In particular, these samples show a higher and narrower K-edge peak with respect to XANES spectra collected on the entire root.

The XANES spectra of rhizosphere materials (Figure 3c) are more pronounced than in the root samples, pointing out a local structure generally more ordered in the soil surrounding the roots. Moreover the spectral features in the rhizosphere are often reproduced in the root samples, as noticed above. Specifically, the XANES spectrum of *Rhiz Euph* sample shows characteristics present both in Zn oxide spectrum (label A), hydrozincite spectrum (labels 2 and 3), and hemimorphite/willemite (label 4). The XANES features labeled as 4 and 5 at the hemimorphite edge white line are present also in the *Rhiz Euph_control* sample. Also the minimum in the hemimorphite spectrum (Figure 3c, label 3) comes in agreement with the valley observed in the *Rhiz Euph_control* sample. On the contrary, the major features observed in the XANES spectrum of willemite are absent in this rhizosphere sample (Figure 3c, labels D and E). The minimum in the hydrozincite and hemimorphite spectrum comes in agreement also in the *Rhiz Euph_CP1* sample.

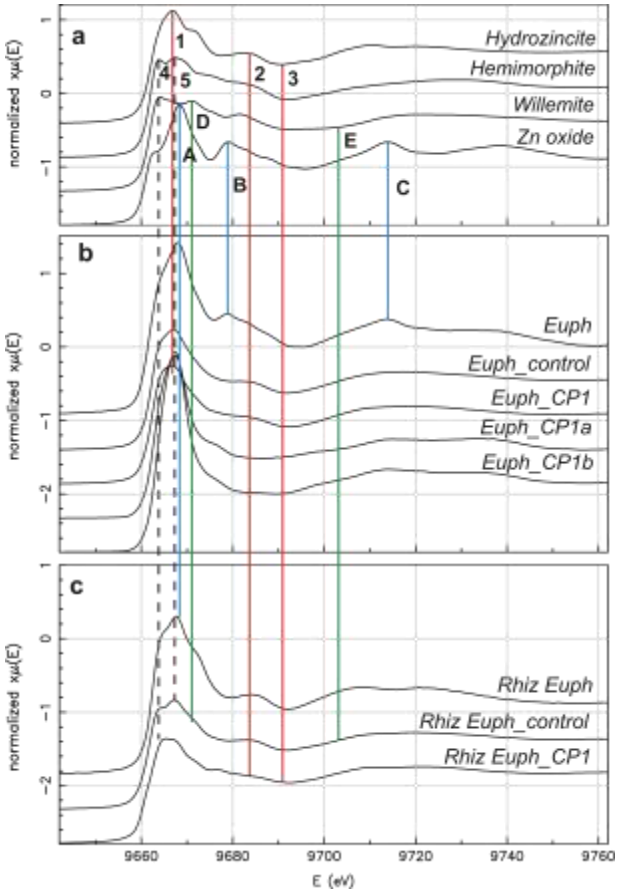

Figure 3. Normalized absorption spectra (α) in the Zn K-edge XANES collected on selected reference compounds (a), *E. phytiusa* roots (b) and rhizosphere materials (c), vertically shifted for the sake of clarity. Similar features among root plant samples, rhizosphere materials and reference compunds are highlighted.

The EXAFS region is definitively more suited than XANES for a quantitative analysis to achieve details about average Zn coordination numbers and interatomic distances. The analysis of EXAFS spectra collected on reference compounds (see Table S2) was used to tailor the refinement procedure: the structural results of our standards are in agreement with the available literature data.[48]

The quantitative analysis of the EXAFS spectra was performed on all the investigated root samples (except the *Euph* sample as motivated above). Representative analyses of Zn K-edge EXAFS data are reported in Figures 4a and b: experimental data and best fit curves are presented in k-space (Figure 4a) and real space (Figure 4b). Table 3 shows Zn local structure parameters obtained from plant root samples EXAFS data analysis.

As all the type 2 samples depict similar features in the Zn K edge XANES region, we can safely assume that Zn belongs approximately to the same structure in all of them. The values of the structural parameters reported in Table 3 (*E. pithyusa* - entire root) are obtained averaging the EXAFS data analysis of all the spectra. The uncertainty on the parameters is the standard deviation of the distribution of the results.

The quantitative analysis of the EXAFS spectra measured on the entire roots demonstrates Zn being approximately 5-coordinated to oxygen around R_{ZnO} = 2.01 Å. A weak (but statistically significant) next neighbour Zn-Si shell is found around R_{ZnSi} = 2.97 Å having a coordination number N_{ZnSi} = 1.6. This demonstrates that ZnO5 polyhedra are likely part of a silicate network instead of being dispersed into an organic matrix. In some cases (*Euph_A2*, *Euph_B1*), a third shell Zn-Zn was also recognized around R_{ZnZn}= 3.8 Å with a relatively high coordination number N_{ZnZn}= 2.7 suggesting a mechanism causing the aggregation of Zn in Zn-rich regions instead of a homogeneous dispersed.

EXAFS analysis from epidermis (*Euph_CP1b*) and inner part of the root (*Euph_CP1a*) reveals significant differences: the *Euph_CP1b* data fit point out a first Zn-O shell (R ~2 Å), and a second Zn-Si shell (R ~ 3 Å). For the inner part of the root (*Euph_CP1a*), the best fit confirms a nearest neighbour Zn-O shell (R ~ 2 Å), but the next neighbour structure depicts heavy ions, and the best fit suggests a second Zn-Zn shell at about 3.2 Å, and a third Zn-Zn shell at about 3.4 Å, while Zn-Si neighbours were not observed.

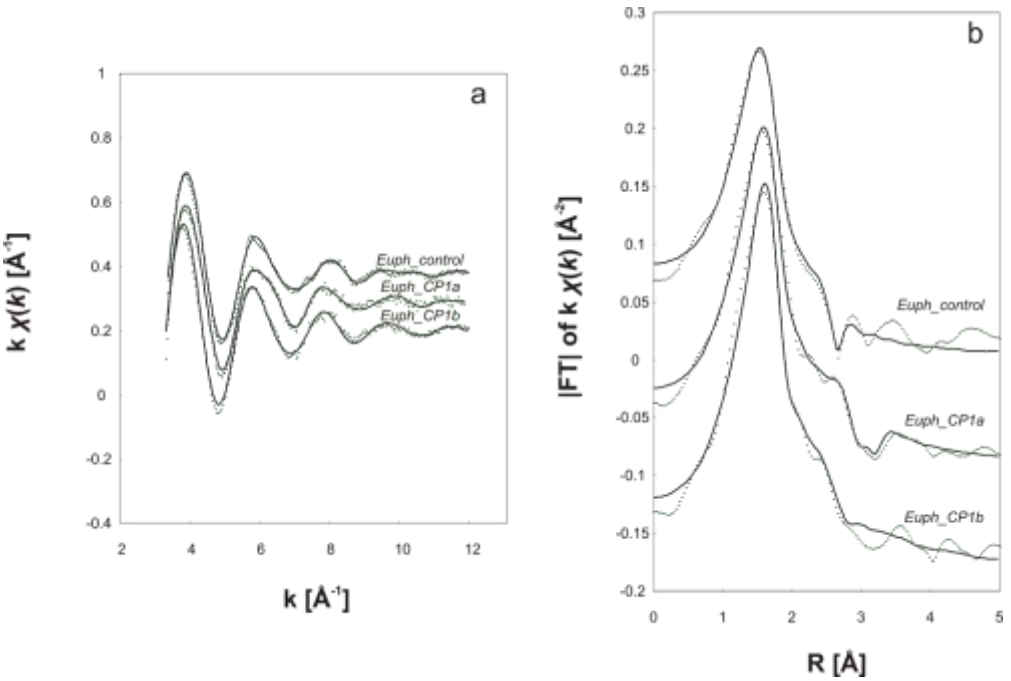

Figure 4. Experimental data (points) and best fits (full lines) of selected root samples EXAFS spectra (a), and Fourier transforms of EXAFS spectra (b).

Table 3. Fit parameters for EXAFS analysis

	CN	R (Å)	σ^2 (x10^{3}Å)	R^2
***E. pithyusa*- entire root (N = 5)[a]**				~ 0.02
ZnO	4.9±0.6	2.01±0.01	9±2	
ZnSi	1.6±0.8	2.97±0.04	12±5	
ZnZn	2.7±0	3.85±0.02	19±3	
Euph_CP1a				0.02
ZnO	4.5(5)	2.01(1)	7.5(5)	
ZnZn	1*	3.24(1)	5.3(6)	
ZnZn	2*	3.41(1)	10(1)	
Euph_CP1b				0.02
ZnO	4.6(5)	2.03(1)	5.9(4)	
ZnSi	0.9(1)	3.02(1)	8(2)	

[a]mean values and standard deviation of *Euph_control*, *A2*, *B1*, *MB*, and *Euph_CP1* samples. N = number of samples.
CN = coordination number; R = interatomic distance; σ^2 = Debye-Waller; R^2 = best fit factor.
The number in brackets indicates the uncertainty on the last digit of the refined parameters.

Figures 5a and b show selected experimental rhizosphere Zn-edge EXAFS spectra, and Fourier transforms (FT), respectively. A comparison between EXAFS spectra of root samples and those of rhizosphere solid materials indicates a more ordered structural environment of Zn in these materials

with respect to root samples. Despite that, quantitative EXAFS analysis of rhizosphere samples was not carried out, because the presence of more phases in the studied samples (also see description of XANES spectra) does not allow a reliable refinement due to the many parameters that must be considered.

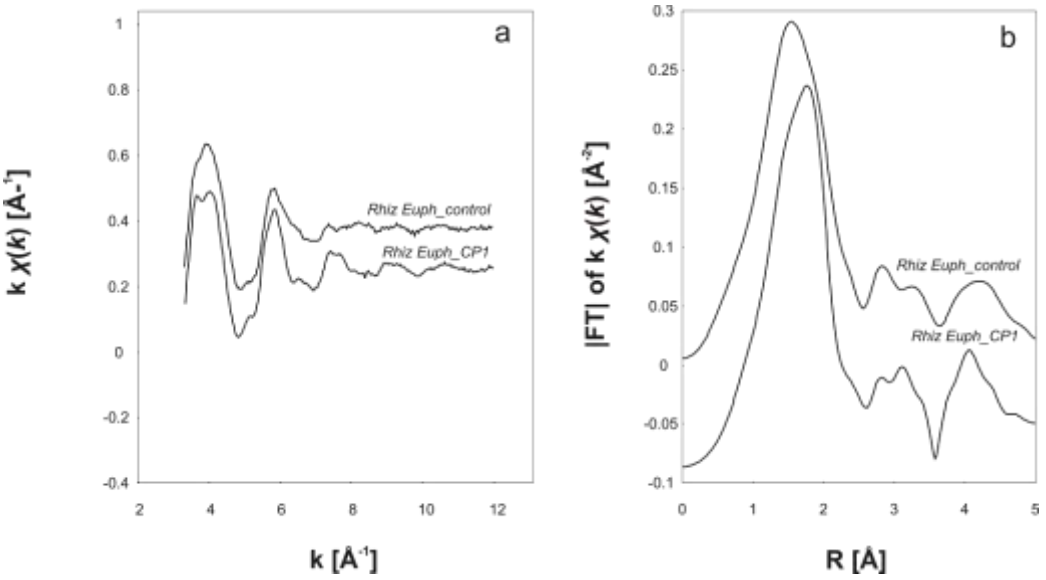

Figure 5. (a) Experimental rhizosphere Zn-edge EXAFS oscillation functions k χ(k) spectra, and Fourier transforms of EXAFS spectra.

4. Discussion

In heavy metal stressed soils, the key parameter for plant growth is not the total amount of metals and metalloids, but rather their availability for the biosphere.[49] For biotechnological purposes, heavy metal bioavailability can be modified in different ways: 1) plant activity influences trace elements speciation by variations in pH, pCO_2, pO_2, redox potential, organic ligand concentrations, and microbial biomass;[49-51] 2) rhizosphere microorganisms, especially mycorrhizal fungi, can increase the plant tolerance against abiotic stress and stimulate plant,[52] and eventually can form substances, such as glomaline, deposited within hyphal cell wall, that are potential chelating substances;[53] 3) plant growth can benefit from addition of bacterial inocula, because they speed up regeneration processes and humification in the soil, and may provide desired metabolic functions

through a specifically targeted bioaugmentation;[54] bacteria also secrete extracellular polymeric substances involved in bioprecipitation[55] and metal binding, decreasing their bioavailability and toxicity.[56]

It is well known that Zn, and other metals such as Cu, Ni and Cr, are stored in plant roots as metal-organic complexes such as Zn-oxalate and Zn-phosphate,[24] Zn-phytate,[21] Zn-histidine,[22] Zn-phosphate, Zn-malate, and Zn-citrate.[23] More rarely it was observed that metals are bound to inorganic species (Zn-Ca phyllo manganate[7]). Neumann and Zur Nieden[25] and Neumann and De Figueiredo,[57] using Environmental Sensitivity Index (ESI) mapping and Electron Energy Loss Spectroscopy (EELS), showed that heavy metal tolerant *Cardaminopsish allery* is able to take up Zn in invaginations and vacuolar vesicles in the form of a Zn-silicate. In the vacuoles, the unstable Zn-silicate is degraded, forming SiO_2 precipitates, while the released Zn is bound to an unknown partner.

Specifically to *E. pithyusa,* we observed that Si and Al are mainly concentrated into the epidermis of the roots (see elemental map acquired by SEM, Figure 1, and LEXRF maps, Figure 2). XRD analysis (Figures S2a and b) reveals the presence of crystalline SiO_2 both in the epidermis of the plant roots and in the inner part, suggesting that silica biomineralization could occur inside the plant roots due to adsorption of silicic acid by the roots.[58,59] XANES spectra of plant roots and rhizosphere materials are characterized by similar features, indicating that plants absorb Zn mainly in its mineralogical phase rather than dissolving it. This is definitively evident in the case of *Euph* sample in which a large fraction of ZnO in the rhizosphere corresponds to a large fraction of ZnO into the root body. Moreover, the LEXRF mapping (Figure 2) combined with results from EXAFS analysis (Table 4) rule out an organic binding complex, and show that *E. pithyusa* uses Si to bind Zn forming an amorphous Zn-silicate. This process is intrinsically biologically driven, and leads to the decrease of Zn concentration from the epidermis to the internal part of the root (Figure 2), where Zn is bonded to other Zn atoms. When Zn concentration is very high, as in the rhizosphere of *E. pithyusa* collected on the mine tailings at Campo Pisano (sample *Euph_CP1*), the Al-Si rim and Zn-

346 silicate trap are not enough to prevent Zn penetration into the roots, and its concentration results
347 relevant also inside (Figure 2), with no recognizable decrease from the epidermis to the internal part
348 of the root. Thus we argue that this rim acts as a physico-chemical barrier against organic and
349 inorganic stresses, in agreement with other authors.[60]
350 As previously stated, these processes of Zn and Si uptake from soil minerals and formation of new
351 Zn-Si amorphous phase at the rim, and Zn-rich complex in the inner part of the roots are
352 intrinsically driven by the plant. The occurrence of a Zn-silicate biomineralization in the outer rim
353 of *E. pithyusa* root reveals an unexpected use of Si in both rhizosphere mineral evolution and
354 biological regulation of bioavailable Zn. We did not find effects of biopolymers secreted by bacteria
355 on Zn speciation analysis. In our investigated system, we proved that Zn bioavailability is ruled
356 only by plant processes independent by microbial activity, while soil microbial properties such as
357 N-fixation were improved by benefit from microbial inocula (see Sprocati et al, 2014). The results
358 of this study seem to suggest that an effective strategy of revegetation with *E. pithyusa* in this kind
359 of soils is to simply provide the optimum conditions (nutrient supply and adequate soil
360 environment) for its basic metabolic functions. The plant has its own "built in" mechanism for
361 heavy metal tolerance, and does not seem to need specific external aids to this end. In a broader
362 perspective, the understanding of the molecular mechanism ruling Zn silicate biomineralization
363 could lead to a step forward in phytoremediation technologies. This study reinforces the concept
364 that understanding microscopic processes ruling bio-geosphere interaction may open new
365 possibilities to develop bioremediation techniques.
366

367 **Associated content**

368 **Supporting Information**

369 Additional details on description of the studied area and results. This material is available free of
370 charge via the Internet at http://pubs.acs.org.

Author information

Corresponding author

*phone +39 070 675 7720. E-mail gbgiudic@unica.it

Acknowledgments

This research was carried out in the framework of the European project UMBRELLA (FP7-ENV-2008-1 no. 226870). Additional funding was provided by Regione Sardegna (Biophyto and SMERI projects), and MIUR (PRIN 2010-2011 Minerals-biosphere interaction).

References

(1) Lucas Y. The role of plants in controlling rates and products of weathering: importance of biological pumping. *Annu. Rev. Earth Planet. Sci.* **2001**, 29:135–63

(2) Skinner, H. C. W.; Jahren, A. H. Biomineralization. In *Treatise on Geochemistry*, Volume 8. Schlesinger W. H. Ed. Executive Editors: Heinrich D. Holland and Karl K. Turekian. pp. 682. ISBN 0-08-043751-6. Elsevier, 2003, p.117–184.

(3) He, H.; Veneklaas, E. J.; Kuo, J.; Lambers, H. Physiological and ecological significance of biomineralization in plants. *Trends Plant Sci.* **2014**, *19* (3),166–174.

(4) Shah, F. U. R.; Ahmad, N.; Masood, K. R.; Peralta-Videa, J. R.; Ahmad, F. D. Heavy metal toxicity in plants. In *Plant Adaptation and Phytoremediation*; Ashraf, M., Ozturk, M. Ahmad, M. S. A. Eds.; Springer, Dordrecht, Heidelberg, London, New York 2010; pp 71–98.

(5) Gardea-Torresdey, J. L.; Arteaga, S.; Tiemann, K. J.; Chianelli, R.; Pingitore, N.; Mackay, W. Absorption of copper(II) by creosote bush (Larrea tridentata): Use of atomic and x-ray absorption spectroscopy. *Environ. Toxicol. Chem.* **2001,** *20* (11), 2572–2579.

(6) Gardea-Torresdey, J. L.; Videa, J. R. P.; Rosa, G. D.; Parsons, J. Phytoremediation of heavy metals and study of the metal coordination by X-ray absorption spectroscopy. *Coord. Chem. Rev.* **2005**, *249* (17-18), 1797–1810.

(7) Lanson, B.; Marcus, M. A.; Fakra, S.; Panfili, F.; Geoffroy, N.; Manceau A. Formation of Zn–Caphyllomanganate nanoparticles in grass roots. *Geochim. Cosmochim. Acta* **2008**, *72*, 2478–2490.

(8) Rodríguez, N.; Menéndez, N.; Tornero, J.; Amils, R.; de la Fuente, V. Internal iron biomineralization in Imperata cylindrica, a perennial grass: chemical composition, speciation and plant localization. *New Phytol*. **2005**, *165* (3), 781–789.

(9) Sarret, G.; Isaure, M. -P.; Marcus, M. A.; Harada, E.; Choi, Y. -E.; Pairis, S.; Fakra, S.; Manceau, A. Chemical forms of calcium in Ca,Zn- and Ca,Cd containing grains excreted by tobacco trichomes. *Can. J. Chem.* **2007**, *85*, 738–746.

(10) Prasad, M. N. V.; Freitas, H. M. de O. Metal hyperaccumulation in plants - Biodiversity prospecting for phytoremediation technology. *Electron. J. Biotechn*. **2003**, *6* (3), 285-321.

(11) Ghosh, M.; Singh, S. P. A Review on Phytoremediation of Heavy Metals and Utilization of Its Byproducts. *Appl. Ecol. Environ. Res.* **2005**, *3* (1), 1–18.

(12) McCutcheon, S. C.; Schnoor J. L. Overview of Phytotransformation and Control of Wastes. In *Phytoremediation: Transformation and Control of Contaminants.* McCutcheon, S. C., Schnoor, J. L., Eds; John Wiley & Sons, Inc. 2004.

(13) Salt, D. E.; Smith, R. D.; Raskin, I. Phytoremediation. *Annu. Rev. Plant Phys.* **1998**, *49*, 643–668.

(14) Wójcik, M.; Sugier, P.; Siebielec, G. Metal accumulation strategies in plants spontaneously inhabiting Zn-Pb waste deposits. *Sci.Total Environ.*, 2014, 487, 313–322.

(15) González, R. C.; González-Chávez, M. C. A. Metal accumulation in wild plants surrounding mining wastes, *Environ. Pollut.*, **2006**, *144* (1), 84–92.

(16) Sprocati, A. R.; Alisi.; Pinto, V.; Montereali, M. R.; Marconi, P.; Tasso, F.; Turnau, K.; De Giudici, G.; Goralska, K.; Bevilacqua, M.; Marini, F.; Cremisini, C. Assessment of the applicability of a "toolbox" designed for microbially assisted phytoremediation: the case study at Ingurtosu mining site (Italy). *Environ Sci. Pollut. Res. Int.* **2014**, *21*(11), 6939–6951.

(17) Kothe, E.; Büchel, G. UMBRELLA: Using MicroBes for the REgulation of heavy metaL mobiLity at ecosystem and landscape scAle (Editorial). Environ. Sci.Pollut. R. 2014, 21 (11), 6761–6764.

(18) Teixeira, C.; Almeida, C. M. R.; Nunes da Silva, M.; Bordalo, A. A.; Mucha, A. P. Development of autochthonous microbial consortia for enhanced phytoremediation of salt-marsh sediments contaminated with cadmium. *Sci. Total Environ.* **2014**, *493*, 757–765.

(19) Lombi, E.; Susini, J. Synchrotron-based techniques for plant and soil science: opportunities, challenges and future perspectives. *Plant Soil* **2009**, *320*, 1–35.

(20) Sarret, G.; Pilon Smits, E.A.H.; Castillo Michel, H.; Isaure, M. P.; Zhao, F. J.; Tappero, R. Use of synchrotron-based techniques to elucidate metal uptake and metabolism in plants. *Adv. Agron.* **2013**, *119*, 1–82.

(21) Kopittke, P. M.; Menzies, N. W.; de Jonge, M. D.; McKenna, B. A.; Donner, E.; Webb, R.I.; Paterson, D. J.; Howard, D. L.; Ryan, C. G.; Glover, C. G.; Scheckel, K. G.; Lombi, E. In Situ Distribution and Speciation of Toxic Copper, Nickel, and Zinc in Hydrated Roots of Cowpea. *Plant Physiol.* **2011**, *156* (2), 663–673.

(22) Salt, D. E.; Prince, R. C.; Baker, A. J. M.; Raskin, I.; Pickering, I. J. Zinc Ligands in the Metal Hyperaccumulator *Thlaspi caerulescens* As Determined Using X-ray Absorption Spectroscopy. *Environ. Sci. Technol.* **1999**, *33*, 713-717.

(23) Sarret, G.; Saumitou-Laprade, P.; Bert, V.; Proux, O.; Hazemann, J. L.; Traverse, A.; Marcus, M. A.; Manceau A. Forms of Zinc Accumulated in the Hyperaccumulator *Arabidopsis halleri*. *Plant Physiol*. **2002**, *13*0, 1815–1826.

(24) Straczek, A.; Sarret, G.; Manceau, A.; Hinsinger, P.; Geoffroy, N.; Jaillard, B. Zinc distribution and speciation in roots of various genotypes of tobacco exposed to Zn. *Environ. Exp. Bot.* **2008**, *63*, 80–90.

(25) Neumann, D.; zur Nieden, U. Silicon and heavy metal tolerance of higher plants, *Phytochemistry* **2001**, *56* (7), 685–692.

(26) Wernitznig, S.; Adlassnig, W.; Sprocati, A. R.; Turnau, K.; Neagoe, A.; Alisi, C.; Sassmann, S.; Nicoara, A.; Pinto, V.; Cremisini, C.; Lichtscheidl, I. Plant growth promotion by inoculation with selected bacterial strains versus mineral soil supplements. *Environ. Sci. Pollut. Res. Int.* **2014**, *21* (11), 6877–6887.

(27) Turnau, K.; Przybylowicz, W. J.; Mesjasz-Przybylowicz, J. Heavy metal distribution in Suillus luteus mycorrhizas - as revealed by micro-PIXE analysis. *Nucl. Instrum. Methods B*, **2001**, *181* (1-4), 649-658.

(28) Ardau, C.; Lattanzi, P.; Peretti, R.; Zucca, A. Chemical stabilization of metals in mine wastes by transformed red mud and other iron compounds: laboratory tests. *Environ. Technol.* **2014;** DOI 10.1080/09593330.2014.930515.

(29) De Giudici, G.; Fanfani, L.; Pisu, T.; Zijlstra, J. J. P. Treatment of arsenic-rich mining waste: comparing arsenate binding capacity of Granulated Ferric Hydroxide and Transformed Red Mud. Rendiconti online *Soc. Geol. It.* **2008**, *2*, 1-3.

(30) Liu, Y.; Naidu, R.; Ming, H. Red mud as an amendment for pollutants in solid and liquid phases. *Geoderma* **2011**, *163* (1–2): 1–12.

(31) Ma, Y.; Feng, X. The application of red mud on restoring heavy metal contaminated water and soil. *Adv. Mater. Res.* **2001**, *225–226*, 1262–1265.

(32) Zijlstra, J. J. P.; Bellò, V.; Ruggeri, R.; Teodosi, A. The BAUXSOLTM Technology: An innovative solution for environmental remediation problems. In Cossu, R. and Stegmann R. (eds). *Proceedings Sardinia Tenth International Waste Management and Landfill Symposium*, 2005, 1019 – 1020.

(33) Zijlstra, J. J. P.; Bellò, V.; Collu, L.; Faux, D.; Ruggeri, R. Passive treatment of AMD with a filter of cemented porous pellets of Transformed Red Mud. In: Cidu, R., Frau F. (eds). Proceedings IMWA Symposium Water in Mining Environments, 2007, Italy, pp. 299 – 303. Presscolor, Quartu Sant'Elena, Italy.

(34) Zijlstra, J. J. P.; Dessì, R.; Peretti, R.; Zucca, A. Treatment of percolate from metal sulfide mine tailings with a permeable reactive barrier of transformed red mud. *Water Environ. Res.* **2010**, *82* (4), 319-327

(35) Cidu, R.; Fanfani, L. Overview of the environmental geochemistry of mining districts in southwestern Sardinia, Italy. *Geochem.: Explor., Environ., Anal.* **2002,** *2*(3), 243–251.

(36) Cidu, R.; Biddau, R.; Fanfani, L. Impact of past mining activity on the quality of groundwater in SW Sardinia (Italy). *J. Geochem. Explor.* **2009**, *100* (2-3), 125–132.

(37) Kaulich, B.; Bacescu, D.; Susini, J.; David, C.; Di Fabrizio, E.; Morrison, G. R.; Charalambous, P.; Thieme, J.; Wilhein, T.; Kovac, J.; Cocco, D.; Salome, M.; Dhez, O.; Weitkamp, T.; Cabrini, S.; Cojoc, D.; Gianoncelli, A.; Vogt, U.; Podnar, M.; Zangrando, M.; Zacchigna, M.; Kiskinova M. Proc. 8th Int. Conf. X-ray Microscopy IPAP Conf. Series 2006, 7, 22.

(38) Gianoncelli, A.; Morrison, G. R.; Kaulich, B.; Bacescu, D.; Kovac, J. A fast read-out CCD camera system for scanning X-ray microscopy. *Appl. Phys. Lett.* **2006**, *89*: 251117-251119.

(39) Morrison, G.R.; Gianoncelli, A.; Kaulich, B.; Bacescu, D.; Kovac, J. A fast read-out CCD system for configured-detector imaging in STXM. Conf. Proc. Series IPAP 7: 277-379. 2006.

(40) Gianoncelli, A.; Kaulich, B.; Alberti, R.; Klatka, T.; Longoni, A.;, de Marco, A.; Marcello, A.; Kiskinova, M. Simultaneous Soft X-ray Transmission and Emission Microscopy. *Nucl. Instrum. Methods* **2009**, *608* (1), 195–198.

(41) Gianoncelli, A.; Kourousias, G.; Stolfa, A.; Kaulich, B. Recent developments at the TwinMic beamline at ELETTRA: an 8 SDD detector setup for low energy X-ray. *J. Phys. Conf. Ser.* **2013**, *425* (18) pp. 182001.

(42) Sole, A.; Papillon, E.; Cotte, M.; Walter, Ph., Susini, J. A multiplatform code for the analysis of energy-dispersive X-ray fluorescence spectra. *Spectrochim. Acta B* **2007**, *62* (1) 63–68.

(43) Meneghini, C.; Bardelli, F.; Mobilio, S. ESTRA-FitEXA: a software package for EXAFS data analysis. *Nucl. Inst. Methods B* **2012**, *285*, 153–157.

(44) Medas, D.; Lattanzi, P.; Podda, F.; Meneghini, C.; Trapananti, A.; Sprocati, A.; Casu, M. A.; Musu, E.; De Giudici G. The amorphous Zn biomineralization at Naracauli stream, Sardinia: electron microscopy and X-ray absorption spectroscopy. *Environ. Sci. Pollut. R.* **2014**, *21*, 6775-6782.

(45) Tomazic, B.; Nancollas, G. H. The kinetics of dissolution of calcium oxalate hydrates. *J. Crys. Growth* **1979**, *46* (3), 355–361.

(46) Giordani, P.; Modenesi, P.; Treatiach, M. Determinant factors for the formation of the calcium oxalate minerals, weddellite and whewellite, on the surface of foliose lichens. *Lichenologist* **2003** *35*(3): 255–270.

(47) Mimmo, T.; Terzano, R.; Medici, L.; Lettino, A.; Fiore, S.; Tomasi, N.; Pinton, R.; Cesco, S. Interaction of root exudates with the mineral soil constituents and their effect on mineral weathering. EGU General Assembly 2012, held 22-27 April, 2012 in Vienna, Austria., p.11494

(48) ICSD (Inorganic Crystal Structure Database) (2011) http://icsd.ill.eu/icsd/index.php.

(49) Kidd. P. S.; Barceló, J.; Bernal, M. P.; Navari-Izzo, F.; Poschenrieder, C.; Shilev, S.; Clemente, R.; Monterroso, C. Trace element behaviour at the root-soil interface: implications in phytoremediation. *Environ. Exp. Bot.* **2009**, *67* (1), 243–259 .

(50) Martínez-Alcalá, I.; Clemente, R.; Bernal, M. P.. Metal availability and chemical properties in the rhizosphere of *Lupinus albus* L. growing in a high-metal calcareous soil. *Water Air Soil Pollut.*, **2009**, 201, 283–293

(51) Puschenreiter, M.; Schnepf, A.; Millán, I. M.; Fitz, W. J.; Horak, O.; Klepp, J.; Schrefl, T.; Lombi, E.; Wenzel, W. W. Changes of Ni biogeochemistry in the rhizosphere of the hyperaccumulator *Thlaspi goesingense*. *Plant Soil*, **2005**, *271*, 205–218.

(52) Hrynkiewicz, K.; Baum, C. The potential of rhizosphere microorganisms to promote the plant growth in disturbed soils. In *Environmental protection strategies for sustainable development*; Malik, A., Grohmann, E. Eds. Springer, Berlin, 2012, pp 35–64.

(53) Turnau, K.; Ostachowicz, B.; Wojtczak, G.; Anielska, T.; Sobczyk, L. Metal uptake by xerothermic plants introduced into Zn-Pb industrial wastes. *Plant Soil* **2010**, *337* (1-2), 299–311.

(54) Sprocati, A. R.; Alisi, C.; Tasso, F.; Marconi, P.; Sciullo, A.; Pinto, V.; Chiavarini, S.; Ubaldi, C.; Cremisini, C. Effectiveness of a microbial formula, as a bioaugmentation agent, tailored for bioremediation of diesel oil and heavy metal co-contaminated soil. *Process Biochem.* **2012**, *947*(11): 1649–1655.

(55) Rusznyák, A.; Akob, D. M.; Nietzsche, S.; Eusterhues, K.; Totsche, K. U.; Neu, T. R.; Frosch, T.; Popp, J.; Keiner, R.; Geletneky, J.; Katzschmann, L.; Schulze, E. D.; Küsel, K. Calcite biomineralization by bacterial isolates from the recently discovered pristine karstic Herrenberg cave. *Appl. Environ. Microbiol*. **2012**, *78* (4), 1157–1167.

(56) Pulsawat, W.; Leksawasdi, N.; Rogers, P. L.; Foster, L. J. R. Anions effects on biosorption of Mn(II) by extracellular polymeric substance (EPS) from Rhizobium etli. *Biotechnol. Lett.* 2003, *25* (15), 1267–70.

(57) Neumann, D.; De Figueiredo, C. A novel mechanism of silicon uptake. *Protoplasma* **2002**, *220* (1-2), 59–67.

(58) Monje, P. V.; Baran, E. J. Characterization of Calcium Oxalates Generated as Biominerals in Cacti. *Plant Physiol*. **2002**, *128* (2), 2002.

(59) Xu, C. X.; Liu, Y. L. Silicon absorption, transport and accumulation in plants. *Act. Bot. Boreal. Occident. Sin.* **2006,** *26* (5), 1071–1078.

(60) Yoshida, S.; Ohnishi, Y.; Kitagishi, K. Histochemistry of silicon in rice plant III. The presence of cuticle-silica double layer in the epidermal tissue. *Soil Sci.Plant Nutr.* **1962**, *8* (2), 1–5.